Singular Perturbation Control for Vibration Rejection in HDDs Using the PZT Active Suspension as Fast Subsystem Observer

Chee Khiang Pang, *Member, IEEE*, Frank L. Lewis, *Fellow, IEEE*, Shuzhi Sam Ge, *Fellow, IEEE*, Guoxiao Guo, *Senior Member, IEEE*, Ben M. Chen, *Fellow, IEEE*, and Tong Heng Lee, *Member, IEEE*

***Abstract*—Currently, position sensors other than the read/write head are not embedded into current hard disk drives (HDDs) due to signal-to-noise ratio and nanometer resolution issues. Moreover, a noncollocated sensor fusion creates nonminimum phase zero dynamics which degrades the tracking performance. In this paper, the singular perturbation theory is applied to decompose the voice coil motor's (VCM's) and induced PZT active suspension's dynamics into fast and slow subsystems, respectively. The control system is decomposed into fast and slow time scales for controller designs, and control effectiveness is increased to tackle more degrees-of-freedom via an inner loop vibration suppression with measured high-frequency VCM's and PZT active suspension's dynamics from the piezoelectric elements in the suspension. Experimental results on a commercial HDD with a laser doppler vibrometer show the effective suppression of the VCM and PZT active suspension's flexible resonant modes, as well as an improvement of 39.9% in 3σ position error signal during track following when compared to conventional notch-based servos.**

***Index Terms*—Hard disk drives (HDDs), PZT, singular perturbation.**

I. Introduction

In 2006, hard disk drives (HDDs) remain as the mainstream of cheap nonvolatile mass data storage devices. Future mobile devices are still relying on magnetism-based storage methodologies despite facing the renowned superparamagnetic effect by venturing into perpendicular recording technologies. However, improvements in sensor fabrication technologies coupled with low-cost digital signal processors (DSPs) allow high signal-to-noise ratio (SNR), high resolution sensors, and enhanced servo algorithms to be embedded into future HDDs while retaining economic competitiveness. Future HDDs will need strong disturbance rejection capabilities for usage in portable devices which require ultrahigh data capacities and ultrafast data transfer rates.

It is well known from a control theory that extraneous sensors alleviate controllers' orders and improve servo performance. Incorporation of additional sensors for active vibration control in HDDs has been studied in, e.g., [1]–[3] to actively damp the resonant modes of actuators together with position error signal (PES). However, a noncollocated sensor fusion results in nonminimum phase zero dynamics in the closed-loop system which degrades the tracking performance. By using singular perturbation (SP) control [4], [5], [18], we can decompose the plant to be controlled into fast and slow subsystems as well as design their controllers independently for internal stability. In fact, by relaxing the tracking requirement to ensure that the slow dynamics are used for tracking the desired trajectory, we can obtain the minimum phase zero dynamics even with noncollocated actuator-sensor pairs.

In this paper, the rigid and flexible modes of a voice coil motor (VCM), with a mounted PZT-actuated active suspension (or PZT active suspension for short), are decomposed into their slow and fast subsystems in a two time scale framework, respectively. The piezoelectric elements in the PZT active suspension are used as a sensor to detect the high-frequency dynamics of the VCM and PZT active suspension for high-frequency inner loop compensation in the active damping of the flexible resonant modes. This approach is more robust than digital notch filters, and a slow controller design for the rigid body modes used in track-seeking or track-following operation mode is independent of the inner loop controller used for high-frequency vibration control. More importantly, it increases the control effectiveness of the servo system since the flexible modes increase the degrees-of-freedom (DOFs) of the VCM, i.e., more DOFs than the number of control inputs. This systematic procedure also works for general nonlinear HDD models, including pivot friction and flex cable nonlinearities, etc.

In this paper, Section II gives a brief introduction on the SP control theory and its extension to a general linear time-invariant (LTI) mechanical system to obtain fast and slow subsystems with rigid and flexible modes. Section III captures the experimental frequency responses to identify the essential state matrices in the subsystems using rigid body and flexible mode dynamics in a VCM with a mounted PZT active suspension. Section IV discusses about the usage of the piezoelectric elements in the PZT active suspension to measure the

Manuscript received April 23, 2006; revised November 17, 2006. Abstract published on the Internet January 27, 2007. This work was supported in part by A*Star SERC under Grant 052 101 0097.

C. K. Pang is with the A*STAR Data Storage Institute, Singapore 117608, and also with the Department of Electrical and Computer Engineering, National University of Singapore, Singapore 117576 (e-mail: ckpang@nus.edu.sg).

F. L. Lewis is with the Advanced Controls and Sensors Group, Automation and Robotics Research Institute, The University of Texas at Arlington, Arlington, TX 76019 USA.

S. S. Ge, B. M. Chen, and T. H. Lee are with the Department of Electrical and Computer Engineering, National University of Singapore, Singapore 117576.

G. Guo is with the A*STAR Data Storage Institute, Singapore 117608.

Color versions of one or more of the figures in this paper are available online at http://ieeexplore.ieee.org.

Digital Object Identifier 10.1109/TIE.2007.893074

high-frequency dynamics of a VCM and suspension. Section V designs the corresponding fast and slow controllers for inner and outer loop compensation. The performance of the proposed control scheme is verified with simulation and experimental results and is discussed in Section VI. Conclusions and future work directions are summarized in Section VII.

II. Singular Perturbation Theory (SPT) for LTI Mechanical Systems

For a general LTI mechanical system, its state space representation can be written as

$$\begin{bmatrix} \dot{x}_{\mathrm{R}} \\ \varepsilon \dot{x}_{\mathrm{F}} \end{bmatrix} = \begin{bmatrix} A_{\mathrm{RR}} & A_{\mathrm{RF}} \\ A_{\mathrm{FR}} & A_{\mathrm{FF}} \end{bmatrix} \begin{bmatrix} x_{\mathrm{R}} \\ x_{\mathrm{F}} \end{bmatrix} + \begin{bmatrix} B_{\mathrm{R}} \\ B_{\mathrm{F}} \end{bmatrix} u_V \tag{1}$$

and the output y of the mechanical system is given by

$$y = \begin{bmatrix} C_{\mathrm{R}} & C_{\mathrm{F}} \end{bmatrix} \begin{bmatrix} x_{\mathrm{R}} \\ x_{\mathrm{F}} \end{bmatrix}. \tag{2}$$

$[\, x_{\mathrm{R}}^T \quad x_{\mathrm{F}}^T \,]^T$, u_V, and y are the states, control input, and output of the mechanical system, respectively, and ε is a small positive scalar $(0 < \varepsilon \ll 1)$ which represents that the flexible mode dynamics are much faster than the rigid body modes. In fact, ε can be used as a tuning parameter such that the rigid body dynamics x_{R} are developed along a time scale t while the flexible mode dynamics x_{F} are developed along the time scale $\tau = t/\varepsilon$ to yield $d(x_{\mathrm{F}})/d\tau = \varepsilon \dot{x}_{\mathrm{F}}$.

The SP design technique involves rewriting the system dynamics into slow and fast subsystems assuming that they operate on different time scales and which make them independent of each other [4], [5]. This technique allows an independent controller design while increasing the control effectiveness which is essential for controlling more DOFs than dimensions of control inputs. In the following section, we shall decompose the general LTI mechanical system into slow (denoted by superscript $^-$) and fast (denoted by superscript $^\sim$) subsystems, respectively.

A. Slow Subsystem

The slow subsystem dynamics are obtained by setting $\varepsilon = 0$ together with the corresponding slow variables. As such, the slow manifold equation is obtained by

$$\begin{aligned} 0 &= A_{\mathrm{FR}} \bar{x}_{\mathrm{R}} + A_{\mathrm{FF}} \bar{x}_{\mathrm{F}} + B_{\mathrm{F}} \bar{u}_V \\ \therefore\ \bar{x}_{\mathrm{F}} &= -A_{\mathrm{FF}}^{-1} (A_{\mathrm{FR}} \bar{x}_{\mathrm{R}} + B_{\mathrm{F}} \bar{u}_V) \end{aligned} \tag{3}$$

which, in essence, is an algebraic equation. Obviously, A_{FF} is assumed to be invertible which is obtained from the fast subsystem dynamics to be detailed in the next section. Substituting (3) into the top equation of (1), the slow system dynamics can be obtained as

$$\dot{\bar{x}}_{\mathrm{R}} = \left(A_{\mathrm{RR}} - A_{\mathrm{RF}} A_{\mathrm{FF}}^{-1} A_{\mathrm{FR}}\right) \bar{x}_{\mathrm{R}} + \left(B_{\mathrm{R}} - A_{\mathrm{RF}} A_{\mathrm{FF}}^{-1} B_{\mathrm{F}}\right) \bar{u}_V. \tag{4}$$

Similarly, substituting (3) into (2), the output of the slow subsystem $\bar{y}_V$ is then given by

$$\bar{y}_V = \left(C_{\mathrm{R}} - C_{\mathrm{F}} A_{\mathrm{FF}}^{-1} A_{\mathrm{FR}}\right) \bar{x}_{\mathrm{R}} - C_{\mathrm{F}} A_{\mathrm{FF}}^{-1} B_{\mathrm{F}} \bar{u}_V. \tag{5}$$

It is worth noting that there is a direct feedthrough term in the slow subsystem which reduces the relative degree (properness) of the slow subsystem and must be confronted in any SP-based design.

B. Fast Subsystem

In deriving the fast subsystem dynamics, we work in the fast time scale with $\tau = t/\varepsilon$, and hence, the top equation in (1) can be written as

$$\frac{d}{d\tau} x_{\mathrm{R}} = \varepsilon \dot{x}_{\mathrm{R}} \approx 0 \tag{6}$$

assuming that the rigid body does not change much in the fast time scale, and hence, $\tilde{x}_{\mathrm{R}} \approx 0$.

Similarly, the bottom equation in (1) can be written as

$$\begin{aligned} \varepsilon \frac{d}{dt} x_{\mathrm{F}} &= \frac{d}{d\tau} (\bar{x}_{\mathrm{F}} - \tilde{x}_{\mathrm{F}}) \\ &= A_{\mathrm{FR}} \bar{x}_{\mathrm{R}} + A_{\mathrm{FF}} (\bar{x}_{\mathrm{F}} + \tilde{x}_{\mathrm{F}}) + B_{\mathrm{F}} (\bar{u}_V + \tilde{u}_V). \end{aligned} \tag{7}$$

Using the slow manifold equation in (3), the state equation of the fast dynamics can be obtained as

$$\frac{d}{d\tau} \tilde{x}_{\mathrm{F}} = A_{\mathrm{FF}} \tilde{x}_{\mathrm{F}} + B_{\mathrm{F}} \tilde{u}_V \tag{8}$$

with the assumption that $d(\bar{x}_{\mathrm{F}})/d\tau = 0$ or the slow parts of the flexible modes do not vary much in the fast time scale.

The output of the fast subsystem is, hence, given by

$$\tilde{y}_V = C_{\mathrm{F}} \tilde{x}_{\mathrm{F}}. \tag{9}$$

III. System Identification

In a conventional HDD, the VCM is the only actuator with the R/W (read/write) head mounted on the tip of the suspension. Typically, a VCM can be represented by rigid body dynamics (low-frequency double integrator) and flexible mode dynamics (high-frequency resonant modes, including suspension modes), respectively. In this section, we shall identify the state matrices required for subsystem decomposition using experimental frequency responses.

A picture of a typical VCM, with a mounted PZT active suspension, is shown in Fig. 1. For our application, A_{RF} is assumed to be negligible as the rigid and flexible modes are mechanically decoupled or the flexible resonant modes are assumed to have little or no induced dynamics on the bulky VCM. Similarly, A_{FR} is also assumed to be negligible as the flexible resonant modes occur at high frequencies where the gain of the rigid body is very small due to at least -40-dB/dec amplitude reduction from its low-frequency double integrator properties. These assumptions are validated prior to using a differential laser doppler vibrometer (LDV), and the experimental procedures are omitted here for brevity.

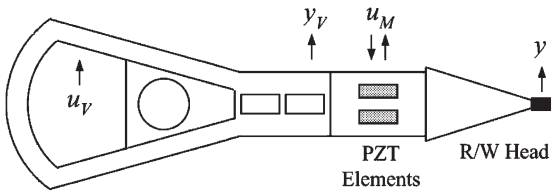

Fig. 1. Drawing of a VCM with a mounted PZT active suspension (not drawn to scale) showing inputs (arrow to actuator) and output or measurement signals (out of actuator), respectively.

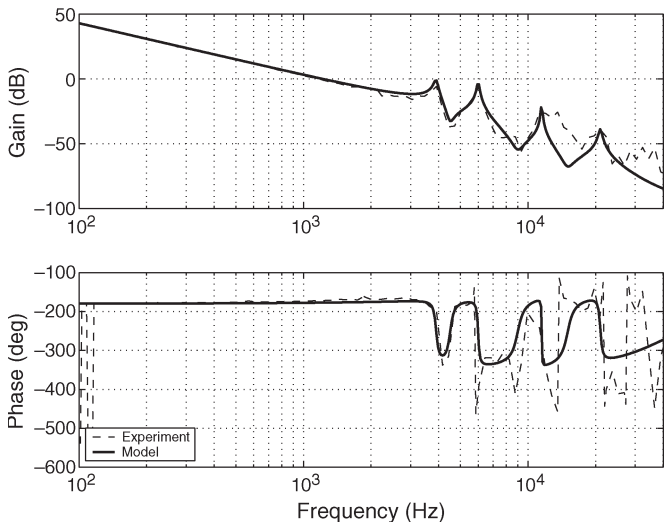

Fig. 2. Frequency response of a transfer function from u_V to y. Both the VCM's and PZT active suspension's flexible resonant modes are excited and identified.

By exciting the VCM at u_V, the frequency response of the VCM, with the PZT active suspension measured from y, is shown in Fig. 2. The identified mathematical model of $y(s)/u_V(s)$ is

$$\frac{y(s)}{u_V(s)} = \frac{2974514.7531}{s^2}\,\frac{s^2+1696s+7.994\times10^8}{s^2+980.2s+6.005\times10^8} \times \frac{s^2+5655s+3.198\times10^9}{s^2+754s+1.421\times10^9}\cdots \times \frac{s^2+9425s+8.883\times10^9}{s^2+361.3s+5.221\times10^9} \times \frac{s^2+2.513\times10^5 s+6.317\times10^{10}}{s^2+3958s+1.741\times10^{10}}. \quad (10)$$

The phase response of the fitted mathematical model is less than exemplary, but is sufficient in picking up the essential rigid and flexible resonant modes, the latter consisting of VCM, and induced PZT active suspension's resonant modes, as shown in Fig. 2. As we are using a gain stabilization in the outer loop at a gain crossover frequency of about 700 Hz and phase compensation of the first flexible resonant mode at 3.9 kHz in the inner loop (to be discussed in detail in Section V) where the experimental and identified model match well, the differences in phase response occurring at higher frequencies are tolerable and do not affect a closed-loop stability.

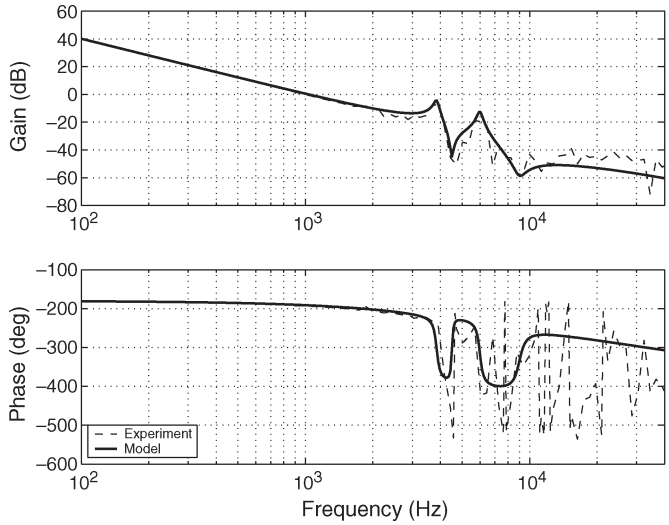

Fig. 3. Frequency response of transfer function from u_V to y_V (i.e., only "E"-block). The VCM has identified double integrator rigid body modes as well as flexible resonant modes at 3.9 and 6.0 kHz.

In the following sections, we shall detail the procedures for determining the state space representation of the VCM with a mounted PZT active suspension in the form of (1) and (2), with the identified experimental frequency responses.

A. Transfer Function Identification

Before we identify the rigid body dynamics, the frequency responses of the VCM from u_V to y_V and the PZT active suspension from u_M to y are shown in Figs. 3 and 4, respectively. As shown in Fig. 3, the VCM itself has identified the rigid body mode (low-frequency double integrator) and flexible body modes (high-frequency resonant modes) at 3.9 and 6.0 kHz, respectively, while the PZT active suspension has flexible body modes at 5.9, 11.5, and 21.0 kHz. It is worth noting that Figs. 3 and 4 serve solely as a reference for modal analysis of the VCM's and PZT active suspension's flexible resonant modes. As such, the phase differences between the experimental and identified mathematical model are considered to be satisfactory and do not affect the stability of the closed-loop system.

When the PZT active suspension is mounted onto the VCM, the proximity in frequencies of the two resonant modes of the VCM and PZT active suspension at 6.0 and 5.9 kHz, respectively, resulted in an overall resonant mode near 6 kHz being observed as shown in Fig. 2, although both resonant modes are excited in that frequency region of 5.9 to 6 kHz during a swept sine identification. As such for simplicity, but without loss of generality, these flexible resonant modes are identified as a common mode at 6 kHz in the compound system $y(s)/u_V(s)$ as shown in Fig. 2 and (10) for SP control.

For our application, the PZT active suspension is employed solely as a sensor and fast subsystem observer to detect high-frequency dynamics of the VCM and PZT active suspension. As such, Fig. 4 serves as a good reference for the sufficiency of a reduced order model to isolate the flexible modes arising from the VCM and PZT active suspension.

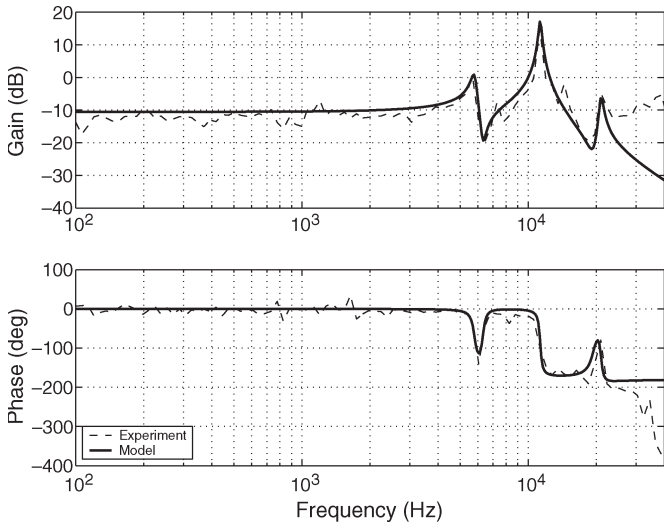

Fig. 4. Frequency response of transfer function from u_M to y. The PZT active suspension has identified flexible body modes at 5.9, 11.5, and 21.0 kHz.

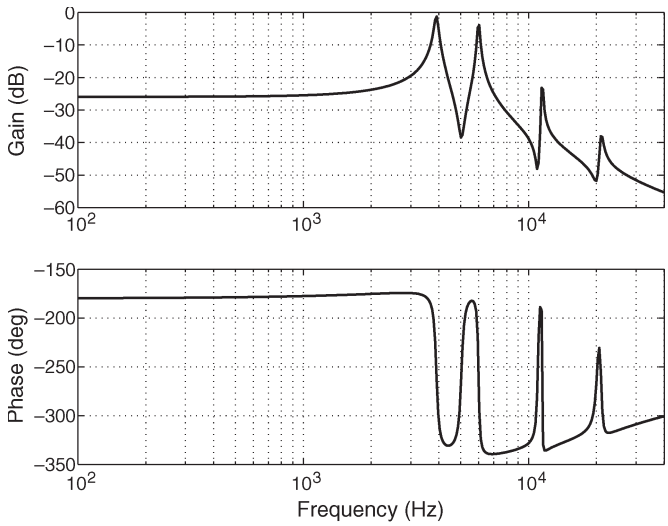

Fig. 5. Frequency response of fast subsystem $\tilde{G}_V$ from $V_{\rm F}(s)$ after decomposition. The flexible resonant modes at natural frequencies 3.9, 6.0 (from VCM and PZT active suspension), 11.5, and 21.0 kHz are captured and retained.

1) Flexible Body: To obtain the flexible body dynamics $V_{\rm F}(s)$ of the VCM with a mounted PZT active suspension, the low-frequency integrators are subtracted from a transfer function $y(s)/u_V(s)$ with a lifted dc gain (to match that in Fig. 2) to form $V_{\rm F}(s)$ given by

$$\begin{aligned} V_{\rm F}(s) = &-355.9008\frac{s+1.421\times10^5}{s^2+980.2s+6.005\times10^8} \\ &\times\frac{s^2+1471s+1.002\times10^9}{s^2+754s+1.421\times10^9}\cdots \\ &\times\frac{s^2+1766s+4.784\times10^9}{s^2+361.3s+5.221\times10^9} \\ &\times\frac{s^2+6860s+1.611\times10^{10}}{s^2+3958s+1.741\times10^{10}} \end{aligned} \tag{11}$$

and $V_{\rm F}(s)$ will be used for identification of the fast subsystem.

2) Rigid Body: As such, the rigid body dynamics $V_{\rm R}(s)$ of the VCM with a mounted PZT active suspension are given by the isolated low-frequency integrators with a lifted dc gain described above [or difference between (10) and (11)] to form

$$V_{\rm R}(s) = \frac{355.9s+5.5\times10^7}{s^2} \tag{12}$$

and $V_{\rm R}(s)$ will be used to identify the slow subsystem in the following section.

B. Subsystem Identification

With the identified flexible body and rigid body dynamics for the VCM with mounted PZT active suspension in (11) and (12), the fast and slow subsystems operating on two different time scales as detailed in Section II earlier can now be formulated, respectively.

1) Fast Subsystem $\tilde{G}_V$: To obtain the fast subsystem state $\tilde{G}_V$ and its space matrix triple $(A_{\rm FF}, B_{\rm F}, C_{\rm F})$, $V_{\rm F}(s)$ is rewritten in state space representation with $x_{\rm F}$ as the state. Obviously, the pair $(A_{\rm FF}, B_{\rm F})$ is stabilizable and $A_{\rm FF}$ is invertible which makes the SP control possible. The frequency response of $\tilde{G}_V$ is shown in Fig. 5. As shown in Fig. 5, the flexible resonant modes at natural frequencies of 3.9, 6.0 (from VCM and PZT active suspension), 11.5, and 21.0 kHz are captured and retained.

2) Slow Subsystem $\bar{G}_V$: Similarly, $V_{\rm R}(s)$ is then rewritten in state space representation with $x_{\rm R}$ as the state to obtain the state space triple $(A_{\rm RR}, B_{\rm R}, C_{\rm R})$. Using (4) and (5), the dynamics of the slow subsystem $\bar{G}_V$ can be obtained in a transfer function form as

$$\begin{aligned} \bar{G}_V &= \frac{\bar{y}_V(s)}{\bar{u}_V(s)} \\ &= \frac{-0.05037s^2+355.9s+5.5\times10^7}{s^2}. \end{aligned} \tag{13}$$

The frequency response of $\bar{G}_V$ is shown in Fig. 6. As shown in Fig. 6, the low-frequency integrators with a lifted dc gain are captured and retained.

It is worth noting from (13) that the introduction of the feedthrough term $C_{\rm F}A_{\rm FF}^{-1}B_{\rm F}$ in (5) makes the slow subsystem $\bar{G}_V$ proper.

IV. Estimating High-Frequency Dynamics

For the SP control to be feasible, the fast dynamics of $\tilde{G}_V$ should be estimated or measured for vibration rejection using an inner loop compensation. This translates directly into a construction of an estimator for state reconstruction or real-time measurements of the VCM's and PZT active suspension's high-frequency dynamics. In this section, we will use the latter by employing the piezoelectric material in the PZT active suspension as a sensor solely to obtain these flexible mode's vibratory signals in both the VCM and PZT active suspension. This is possible as when piezoelectric materials (e.g., PZT elements) are subjected to strain, charges arise on the surface of the material and, hence, setting up an electric field analogous to back electromotive force in electromagnetic systems.

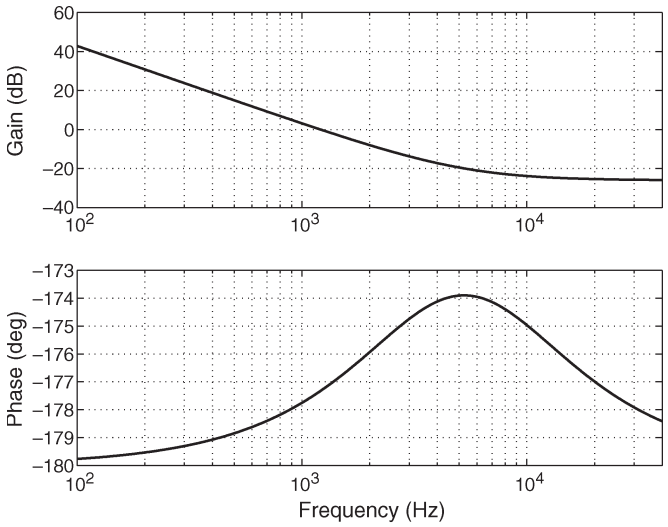

Fig. 6. Frequency response of slow subsystem $\bar{G}_V$ after system decomposition. The low-frequency integrators with a lifted dc gain are captured and retained.

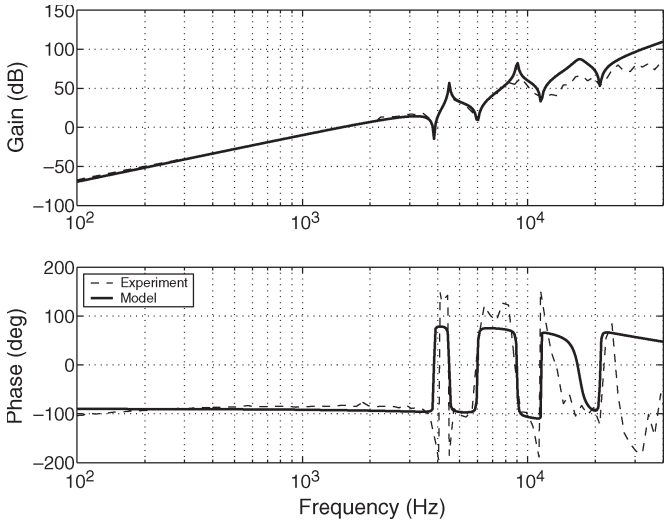

Fig. 7. Frequency response of transfer function from y to u_M using the PZT active suspension as a sensor.

For our experiments, a Brüel and Kjær signal conditioning amplifier of gain 10 and bandpass corner frequencies of 10 Hz and 30 kHz is used. Using a similar methodology to that detailed in [3], a swept sine excitation is injected at u_V while y measured from the LDV is connected to channel 1 and u_M from the PZT active suspension through the amplifier output is connected to channel 2 of the Dynamic Signal Analyzer HP 35670A. The frequency response of the transfer function from y to u_M is measured and shown in Fig. 7. It should be noted that any high-speed low-noise instrumentation amplifiers (e.g., AD524 from analog devices) can be employed here.

As shown in Fig. 7, the estimation is effective at most frequencies and the frequencies of the antiresonant zeros correspond to the natural frequencies of the VCM and PZT active suspension. The online state estimator measured u_M from amplifier to y has differentiator effects and can be identified with the following noncausal transfer function as

$$\frac{u_M(s)}{vy(s)} = 1.2841 \times 10^{-16} s^2 (s^2 + 96.76s + 5.852 \times 10^8) \times \frac{s}{s + 2.513 \times 10^5} \frac{s^2 + 301.6s + 1.421 \times 10^9}{s^2 + 226.2s + 7.994 \times 10^8} \cdots \times \frac{s^2 + 72.26s + 5.221 \times 10^9}{s^2 + 565.5s + 3.198 \times 10^9} \times \frac{s^2 + 1319s + 1.741 \times 10^{10}}{s^2 + 1.068 \times 10^4 s + 1.141 \times 10^{10}} \tag{14}$$

and the high-frequency VCM's and PZT active suspension's dynamics can hence be easily estimated online through a digital inverse of (14) from the output of the amplifier, as detailed in the next section. This method is shown to have high SNR and nanometer resolution estimation, and interested readers are referred to [3] for an in-depth analysis which is not reiterated in this paper.

V. Design of Controllers

According to the SP theory, the overall control signal u_V is given by $u_V = \bar{u}_V + \tilde{u}_V$, where $\bar{u}_V$ and $\tilde{u}_V$ are designed separately using the slow and fast subsystems, respectively. Ensuring that the pair $(A_{\mathrm{FF}}, B_{\mathrm{F}})$ is stabilizable, the composite control u_V results in the following overall state trajectories given by

$$\begin{aligned} x_{\mathrm{R}} &= \bar{x}_{\mathrm{R}} + O(\varepsilon) \\ x_{\mathrm{F}} &= \bar{x}_{\mathrm{F}} + \tilde{x}_{\mathrm{F}} + O(\varepsilon) \end{aligned} \tag{15}$$

where $O(\varepsilon)$ denotes the terms of order ε according to a theorem by Tikhonov [15]. This independent design of two control inputs practically increases the control effectives of the flexible system [14], and the fast control signal $\tilde{u}$ is a boundary layer correction that suppresses the high-frequency vibrations analogous that with sliding mode control.

In fact, this procedure is equivalent to the direct design of a state feedback on the system without any direct or inverse time scaling as we will be using in this section. As such, it possesses better numerical properties as ill-conditioned scenarios (from the large gains and small time constants in HDDs) are commonly encountered during controller synthesis and optimization designs using $\mathcal{H}_2$ or $\mathcal{H}_\infty$ techniques.

The proposed SP control topology using the PZT active suspension as a sensor to determine the VCM's high-frequency dynamics is shown in Fig. 8. The superscripts $^-$, $^\sim$, and * denotes slow subsystems, fast subsystems, and estimates, respectively. The slow controller $(\bar{C}_V)$ and fast controllers $(\tilde{C}_V$ and $\tilde{G}_V^*)$ operate at slow frequency $\bar{f}$ and fast frequency $\tilde{f} = \bar{f}/\varepsilon$, respectively. The fast subsystem dynamics $\tilde{y}_V$ are measured from the PZT active suspension through a signal conditioning amplifier and estimated through $\tilde{G}_V^*$.

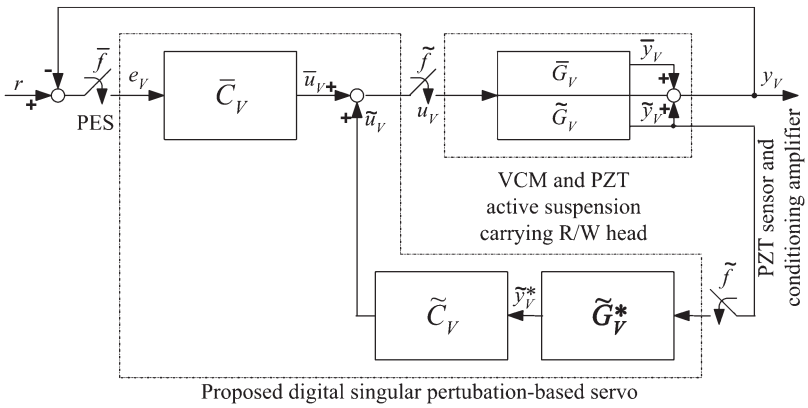

Fig. 8. Block diagram of the proposed SP-based servo system. The slow controller ($\bar{C}_V$) and fast controllers ($\tilde{C}_V$ and $\tilde{G}_V^*$) operate at slow frequency $\bar{f}$ and fast frequency $\tilde{f} = \bar{f}/\varepsilon$, respectively.

A. Fast Subsystem Estimator $\tilde{G}_V^*$

For fast inner loop compensation to be implementable, the high-frequency dynamics of the VCM and PZT active suspension, as mentioned in Section IV, should be available. By designing the fast subsystem estimator $\tilde{G}_V^*$ as the inverse of (14)

$$\begin{aligned}\tilde{G}_V^*(s) = {} & \frac{7.787803 \times 10^{15}}{s^3} \frac{s + 2.513 \times 10^5}{s^2 + 96.76s + 5.852 \times 10^8} \\ & \times \frac{s^2 + 226.2s + 7.994 \times 10^8}{s^2 + 301.6s + 1.421 \times 10^9} \cdots \\ & \times \frac{s^2 + 565.5s + 3.198 \times 10^9}{s^2 + 72.26s + 5.221 \times 10^9} \\ & \times \frac{s^2 + 1.068 \times 10^4 s + 1.141 \times 10^{10}}{s^2 + 1319s + 1.741 \times 10^{10}} \end{aligned} \tag{16}$$

the high-frequency dynamics estimate $\tilde{y}_v^*$ can be obtained online using the output of the amplifier (from measured u_M) as input. This low-pass filter removes much measurement noise from the online estimator which permits a low-order fast controller $\tilde{C}_V$ to be designed.

B. Fast Controller $\tilde{C}_V$

To calculate the fast control signal $\tilde{u}$, we can design any standard linear quadratic Gaussian [20], $\mathcal{H}_2$ or even $\mathcal{H}_\infty$ output feedback controller for high-frequency inner loop compensation. For our design, the nice in phase properties of the PZT active suspension, as shown in Fig. 2, is exploited, and a low-order lead compensator of the form is used

$$\tilde{C}_V = \kappa \frac{s + 6283}{s + 1.257 \times 10^5} \tag{17}$$

as the fast controller $\tilde{C}_V$ with $1 \le \kappa \le 20$. $\tilde{C}_V$ is analogous to a high-gain proportional-derivative control commonly used for controlling robot manipulators [5].

The amount of active high-frequency vibration suppression is increased with a larger κ, but the sensing noise from the PZT elements in the PZT active suspension and conditioning amplifier will be accentuated accordingly and vice versa for a smaller value of κ. As such, κ acts as a compromise to balance between the amount of suppression of high-frequency mechanical vibrations (and inner loop stability) and the amount of sensing noise permeated to and tolerable in the PES. For the rest of our discussions, we have chosen $\kappa = 10$, although the fast controller design can be further optimized if the disturbance and noise spectra entering the servo loop are precisely known [19].

C. Slow Controller $\bar{C}_V$

As the slow subsystem contains mainly of the rigid body modes (low-frequency double integrator), the lag-lead compensator recommended in [3] augmented with a low-pass filter

$$\bar{C}_V(s) = K_V \frac{s + \frac{2\pi f_V}{2\alpha}}{s + 2\pi 10} \frac{s + \frac{2\pi f_V}{\alpha}}{s + 2\alpha 2\pi f_V} \frac{\frac{\alpha\pi f_V}{2}}{s + \frac{\alpha\pi f_V}{2}} \tag{18}$$

where $5 \le \alpha \le 10$ is used. K_V can be calculated by setting $|\bar{C}_V(j2\pi f_V)\bar{G}_V(j2\pi f_V)| = 1$, where $\bar{G}_V$ is the slow subsystem identified in the previous section.

The first lag term of $\bar{C}_V$ is used to increase the low-frequency gain for low-frequency disturbance rejection and tracking accuracy in the slow outer loop. The second term of $\bar{C}_V$ increases the phase margin of the outer open loop to ensure a stability during crossover region and speeding up of the rigid mode in the VCM. An additional low-pass filter is cascaded in the third term of $\bar{C}_V$ to increase the high-frequency roll-off and stability of the stiffened VCM and PZT active suspension due to a reduced relative degree after an inner loop compensation.

The separation of the zeros of $\bar{C}_V$ is increased with a larger α, thereby reducing the low-frequency gain of the integral portion while resulting in a higher corner frequency which increases the phase margin of the outer open loop. f_V is the gain crossover frequency of the compensated VCM open loop and is usually chosen at about one-fifth of the natural frequency of the first major resonant mode of the VCM for stability in digital control of HDD servo systems. For an improved low-frequency performance in disturbance rejection and tracking, $\alpha = 5$ and $f_V = 700$ (the natural frequency of the first resonant mode is at 3.9 kHz) are chosen for our design.

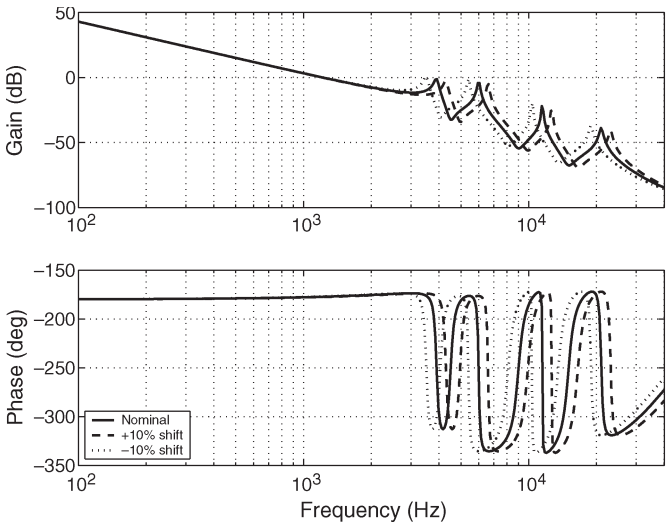

Fig. 9. Frequency response of transfer function from u_V to y with $\pm 10\%$ shift in natural frequencies of the flexible modes.

VI. Performance Evaluation

The proposed SP-based controllers designed in Section V earlier are discretized at a nominal slow sampling frequency $\bar{f}$ of 5 kHz, and $\varepsilon = 0.0625$ is chosen. Due to the parameterization by ε, the fast subsystem estimator $\tilde{G}_V^*$ and fast controller $\tilde{C}_V$ are discretized at a fast sampling frequency $\tilde{f}$ of 80 kHz, where $\tilde{f} = \bar{f}/\varepsilon$. It is interesting to note that in discrete time domain, this formulation is analogous to that of using a multirate digital control with the proposed slow controller $\bar{C}_V$ operating on the measured PES at nominal sampling frequency $\bar{f}$ and fast controllers $\tilde{G}_V^*$ and $\tilde{C}_V$ in inner loop mimicking high sampling frequency $\tilde{f}$ from higher spindle rotation speeds (i.e., more PES data). However, the SP control design methodology is an independent design procedure for subsystems separated in two different time scales which directly ensures a closed-loop stability. The multirate digital control on the other hand relies on small gain theorem to ensure that the fast controller has gain less than or equal to one at all frequencies (e.g., [6]) or sampled-data points analysis in frequency response [7], [8] for stability analysis. In this section, the effectiveness of our proposed SP control scheme is verified with simulation studies and experimental implementations.

A. Simulation Studies

Digital notch filters [21] and phase-stabilized compensators [17] are commonly used by HDD industries to attenuate the gain at natural frequencies of the flexible resonant modes or increase the phase around gain crossover frequency, respectively, for closed-loop stability with the former commonly employed for their structural simplicities and robust properties. To further improve the servo performance of the notch-based servos, multirate digital notch filters are usually designed and operated at a positive integer multiple of nominal sampling frequency. Interested readers are kindly referred to [16] for more details and advantages of digital multirate controllers, or [9] for the HDD track-following servo control benchmark problem where the multirate digital notch filters are employed effectively. For illustration purposes, the fast single-rate and multirate notch-based servos are compared with the proposed SP-based servo.

1) Robustness Analysis: To demonstrate the robustness of the proposed SP-based servo, the natural frequencies of the flexible modes in the VCM and PZT active suspension are perturbed by $\pm 10\%$, as shown in Fig. 9.

The identified vibration and noise models reported in [10] for a servo track writing process with a spindle motor rotating at 5400 r/min (revolutions per minute) are used to emulate input torque disturbances $d_i(s)$, output disturbances $d_o(s)$ and noise sources $n(s)$ of today's high end HDDs, respectively. The transfer functions are given by

$$d_i(s) = \frac{159.9}{s^2 + 113.1s + 3.198 \times 10^5} \tag{19}$$

$$\begin{aligned} d_o(s) = {} & 0.00163 \frac{s^2 - 2.691s + 5.262 \times 10^5}{s^2 + 0.754s + 3.948 \times 10^5} \\ & \times \frac{s^2 - 585.6s + 3.765 \times 10^6}{s^2 + 0.2011s + 1.011 \times 10^6} \cdots \\ & \times \frac{s^2 + 4161s + 2.008 \times 10^7}{s^2 + 245s + 1.668 \times 10^7} \\ & \times \frac{s^2 + 2402s + 5.634 \times 10^8}{s^2 + 477.5s + 5.701 \times 10^8} \end{aligned} \tag{20}$$

and noise source $n(s)$ is of Gaussian distribution with zero mean and a variance of 0.001. Similarly, a noise source of Gaussian distribution with zero mean and a variance of 0.001 is added to mimic the noise in the PZT elements when used as a sensor. This numerical value is close to the experimental PZT noise variance estimated from self-sensing actuation (SSA)—using the PZT active suspension as sensor and actuator simultaneously—as reported in [3].

For comparison purposes, the slow controller $\bar{C}_V$ is discretized via bilinear transformation at $\tilde{f} = 80$ kHz, $\tilde{f}/2 = 40$ kHz, and $\tilde{f}/4 = 20$ kHz, which are termed $\bar{C}_V^1$, $\bar{C}_V^2$, and $\bar{C}_V^4$, respectively. The numerical superscript indicates the ratio of $\tilde{f}$ to the sampling rate at which $\bar{C}_V$ is discretized at.

In designing the digital notch filters $N(z)$, the small damping ratio of each resonant pole of $y(s)/u_V(s)$ in (10) is canceled and set to unity at the same natural frequency. Discretizing the product of the notch filters at a fast sampling frequency $\tilde{f}$ using a pole-zero matching, we obtain $N(z)$ as

$$\begin{aligned} N(z) = {} & 0.22894 \frac{z^2 - 1.895z + 0.9878}{z^2 - 1.656z + 0.7362} \\ & \times \frac{z^2 - 1.774z + 0.9906}{z^2 - 1.45z + 0.6242} \\ & \times \frac{z^2 - 1.235z + 0.9955}{z^2 - 0.1245z + 0.1922} \cdots \\ & \times \frac{z^2 + 0.1556z + 0.9836}{z^2 - 0.9032z + 0.4053}. \end{aligned} \tag{21}$$

Obviously, the gain of $N(z)$ is less than or equal to one at all frequencies required for multirate stability. As such, the fast single-rate notch-based servo controller is given by $\bar{C}_V^1(z)N(z)$. The multirate notch-based servo controllers are $\bar{C}_V^2(z)N(z)$ and $\bar{C}_V^4(z)N(z)$.

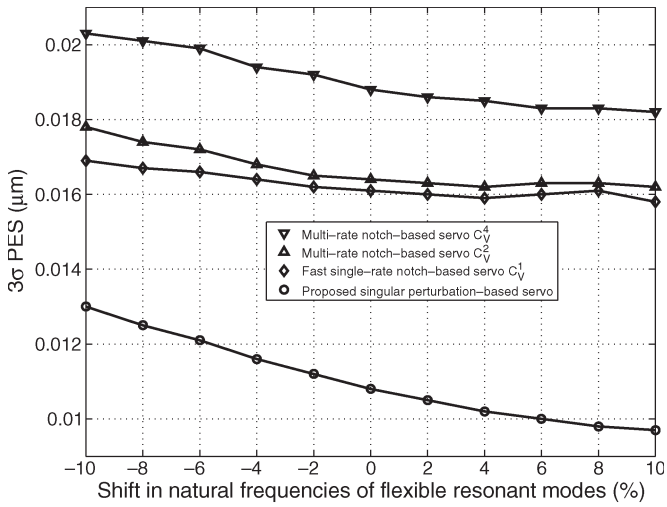

Fig. 10. 3σ PES (μm) versus percentage variation of natural frequency of flexible modes in VCM and PZT active suspension with respect to the nominal frequencies.

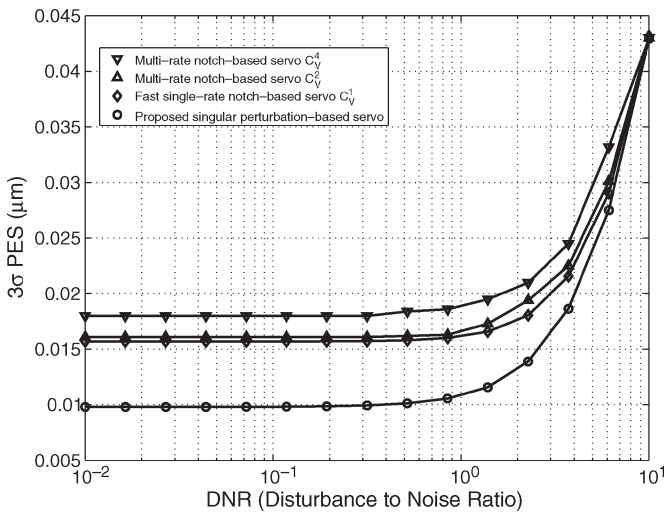

Fig. 11. 3σ PES (μm) versus DNR.

With the designed digital controllers, simulations are then carried out to obtain the 3σ PES with a perturbation of the natural frequencies and are plotted in Fig. 10. As shown in Fig. 10, the SP-based servo is robust to fluctuations in natural frequencies with improved disturbance rejection capabilities at frequency variations occurring in the high-frequency band. An improvement of up to 38.2% in 3σ PES is observed at nominal natural frequencies of the flexible modes.

2) Disturbance-to-Noise Ratio (DNR): In this section, we define a performance index called DNR which is the ratio of output disturbance $d_o(s)$ power to PES measurement noise $n(s)$ power, i.e., DNR $= \sigma_{d_o}^2/\sigma_n^2$. Simulations are then executed to evaluate the proposed SP-based servo as a high-pass filter, which is used for inner loop compensation which is generally undesirable for HDD control (due to high PES sensing noise).

By simulating the DNR from 0.01 to 10 (which translates from a noise level of a hundred times higher than an output disturbance to a tenth smaller), the 3σ PES is plotted in Fig. 11. It can be seen that the proposed SP scheme works well even when the noise level is high, when compared to that of the multirate and fast single-rate notch-based servos.

From the above simulation results, it can be seen that the fast single-rate notch-based servo has better servo performance than their multirate's counterparts due to extra computation cycles. As such, the proposed SP-based servo will be compared to the fast single-rate notch-based servo—or termed conventional notch-based servo for short—in experimental implementations for brevity, but without loss of generality in the rest of this paper.

B. Experimental Implementation

The experimental setup used for verification of our proposed SP-based control scheme is shown in Fig. 12.

For our experiments, the VCM with a mounted PZT active suspension to be controlled is placed on a vibration isolation table. The Polytec PSV-200 SLDV (Scanning LDV) measurement system, consisting of the following: 1) color video camera

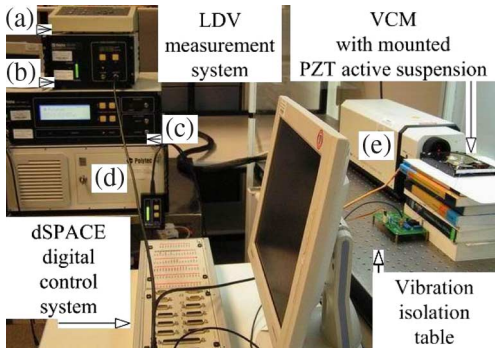

Fig. 12. Experimental setup consisting of VCM with a mounted PZT active suspension to be controlled on a vibration isolation table with the LDV measurement system and dSPACE digital control system.

interface for exact positioning of laser spot, 2) vibrometer controller for displacement and 3) velocity measurements, 4) personal computer (PC) data management system, and 5) the SLDV, as shown in Fig. 12, is used as a displacement transducer to measure the displacement of the R/W head at the tip of the PZT active suspension at a resolution of 0.5 μm/V. The digital controllers designed in Section V are implemented on the dSPACE digital control system using the DS 1103 PPC controller board with an onboard TM320F240 DSP, as well as analogue-to-digital (A/D) and D/A converters of voltage limits at $\pm$10 V. It should be noted that although the SLDV is a capable area scan for modal analysis, only a single point measurement of the displacement of the R/W head at the tip of the PZT active suspension is used.

1) Frequency Responses: The frequency response of the transfer function from u_V to y using the PZT active suspension as a sensor with high-frequency inner loop compensation is shown in Fig. 13. The VCM's flexible modes at 3.9 and 6.0 kHz, and the PZT active suspension's flexible modes at 5.9, 11.5, and 21.0 kHz are effectively damped with a reduced relative degree using the proposed SP-based servo. This further justifies the identification of the VCM's and PZT active suspension's resonant modes at 6.0 and 5.9 kHz, respectively, as a common mode at 6 kHz in the compound system $y(s)/u_V(s)$ in Section III-A previously.

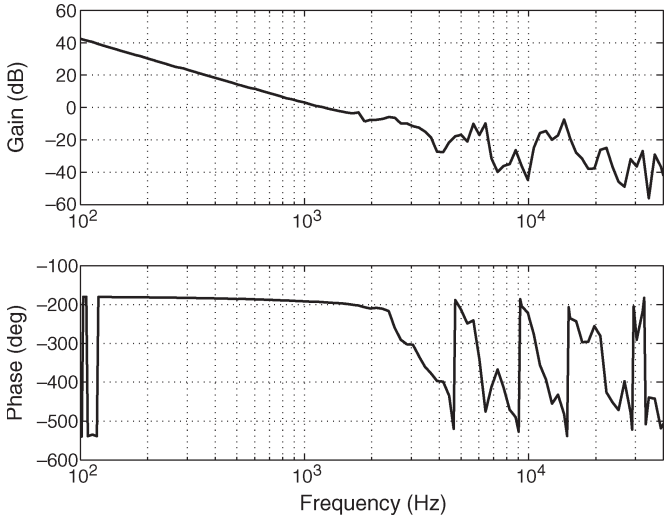

Fig. 13. Frequency response of transfer function from u_V to y using PZT active suspension as a sensor with high-frequency inner loop compensation. The VCM's and PZT active suspension's flexible resonant modes at 3.9, 6.0, 11.5, and 21.0 kHz are effectively damped with a reduced relative degree.

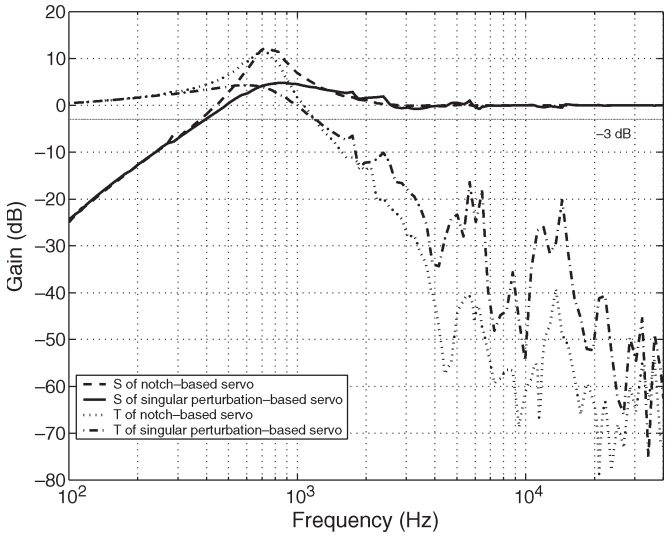

Fig. 14. Frequency response of sensitivity transfer functions with proposed SP-based servo and conventional notch-based servo.

As such, we can expect a possible higher servo bandwidth and low sensitivity with a reduced relative degree. This is verified with the experimental sensitivity transfer functions S of the proposed SP-based servo and conventional notch-based servo, as shown in Fig. 14.

SP-based servo offers stronger vibration suppression capabilities with a higher bandwidth and lower sensitivity such that high-frequency disturbances would not be amplified by the servo loop [11]. However, the complementary sensitivity transfer functions T of the proposed schemes, as shown in Fig. 14, reveal that a smaller roll-off at high frequencies (although at the same closed-loop bandwidth) is obtained for the SP-based servo.

2) Time Responses: While the composite nonlinear feedback (CNF) technique [13] has been shown to reduce overshoot of step responses in HDDs [12], a linear track-following controller is normally employed for short-span seeks in current

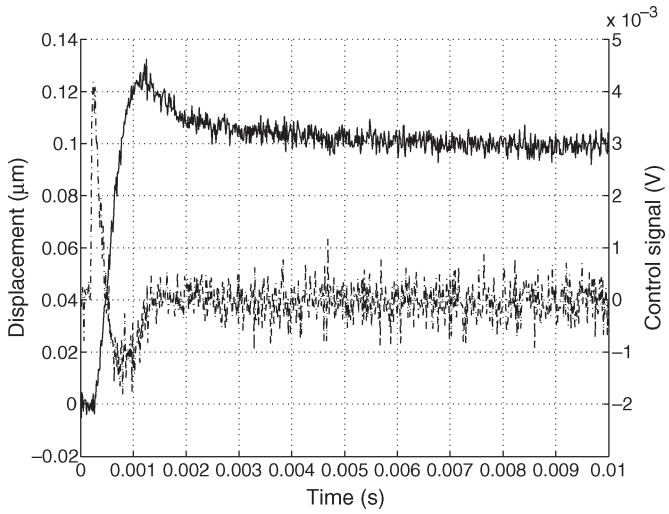

Fig. 15. Experimental step response using the conventional notch-based servo. Solid: displacement measured at tip of PZT active suspension. Dashed–dotted: control signal.

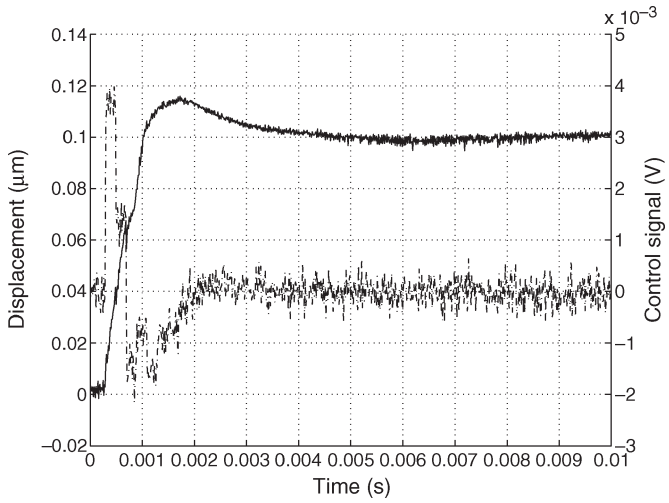

Fig. 16. Experimental step response using the proposed SP-based servo. Solid: displacement measured at tip of PZT active suspension. Dashed–dotted: control signal.

HDDs. For comparison purposes the gain crossover frequencies of both linear track-following controllers for conventional notch-based servo and proposed SP-based servo are set at 700 Hz. The experimental step responses of 0.1 μm using the conventional notch-based servo and the proposed SP-based servo are shown in Figs. 15 and 16, respectively. The slow control signal $\bar{u}_V$ and fast control signal $\tilde{u}_V$ are shown in Fig. 17.

As shown in Figs. 15 and 16, the induced oscillations using the proposed SP-based servos are also highly suppressed by the fast control signal $\tilde{u}_V$. However, the SP-based servo offers a smaller overshoot due to an active vibration control, but a slower seek, and settling time is traded off. This is expected as the tracking requirements are relaxed in an SP framework [5] and tracking is done by the slow subsystem (hence rigid body modes). Also, a fast inner loop active vibration control results in a phase reduction from 2 to 3.9 kHz where the first resonant mode of the VCM occurs, as shown in Figs. 2 and 13. This translates directly into a delay which results in a slower seek

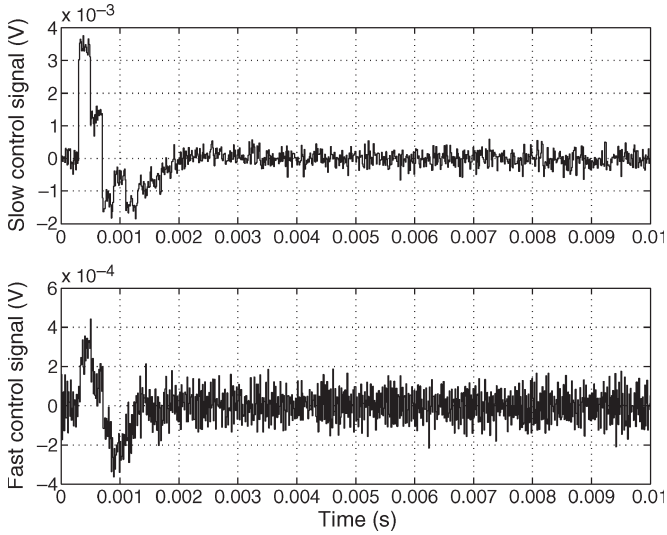

Fig. 17. Control signals using the proposed SP-based servo. Top: slow control signal $\bar{u}_V$. Bottom: fast control signal $\tilde{u}_V$.

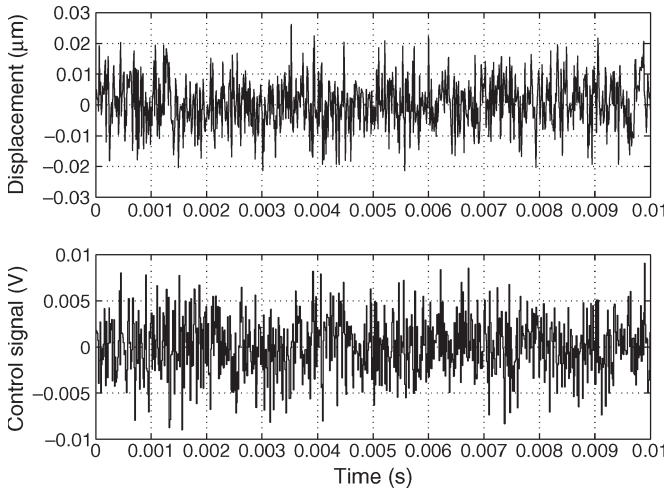

Fig. 18. Experimental PES y measured with LDV using the conventional notch-based servo. Top: displacement measured at tip of PZT active suspension. Bottom: control signal. A 3σ PES of 0.0248 μm is observed.

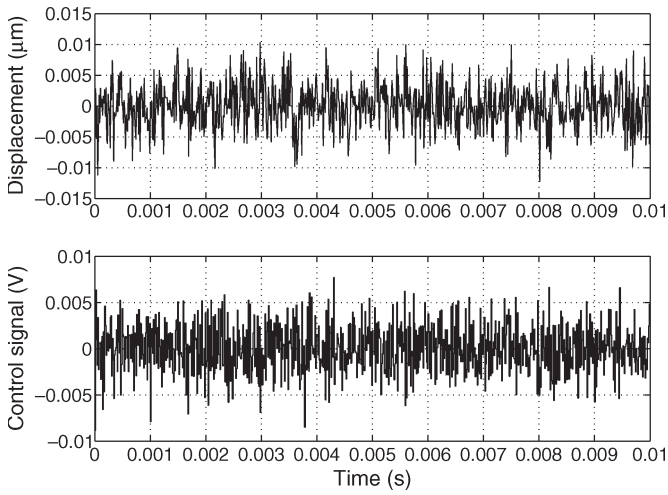

Fig. 19. Experimental PES y measured with LDV using the proposed SP-based servo. Top: displacement measured at tip of PZT active suspension. Bottom: control signal. A 3σ PES of 0.0149 μm is observed.

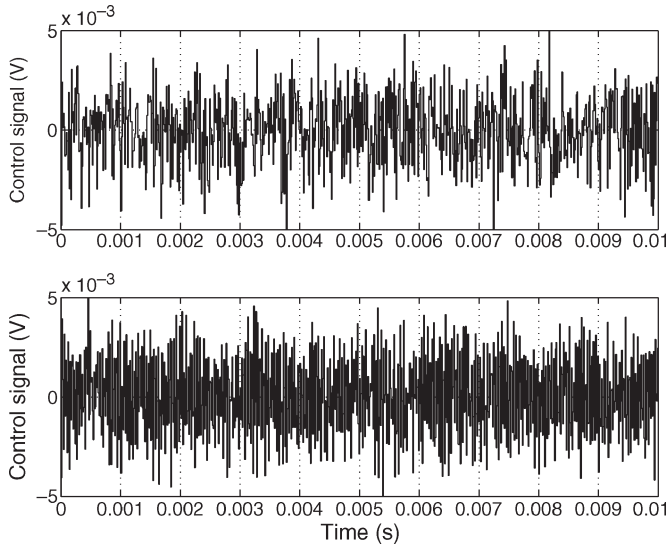

Fig. 20. Control signal using the proposed SP-based servo. Top: slow control signal $\bar{u}_V$. Bottom: fast control signal $\tilde{u}_V$.

response. However, it should be noted that a much higher gain crossover frequency (corresponding to faster seek and settling times) can be designed and achieved for the proposed SP-based servo as the first in-plane resonant mode is well-damped, as shown in Fig. 13 earlier.

Next, to mimic the effects of disturbance and noise sources during track-following mode, the vibration models described earlier in [10] are injected into the closed-loop systems during an experiment. The experimental PES y measured with LDV using the conventional notch-based servo and the proposed SP-based servo are shown in Figs. 18 and 19, respectively. The corresponding experimental slow control signal $\bar{u}_V$ and fast control signal $\tilde{u}_V$ are shown in Fig. 20. An improvement of the experimental 3σ PES from 0.0248 to 0.0149 μm (39.9%) is observed. The 39.9% improvement in the experimental implementation is superior to the 38.2% obtained during the simulation studies as the experiment was conducted on a VCM with a mounted PZT active suspension, employing the PZT elements in the PZT active suspension solely as a sensor. As such, the extraneous bridge circuit and its digital inverse reported in [3] are not applicable, resulting in an effective reduced variance of PZT sensor noise (less than 0.001 used in simulation studies) and, hence, a reduced noise power entering the SP-based servo loop.

The histograms of the above PES data are plotted in Fig. 21, revealing a tighter tolerance and much reduction in variance of the PES.

VII. Conclusion

In this paper, an SP controller design method has been proposed for a stronger vibration suppression in the VCM and PZT active suspension using the piezoelectric elements in the suspension as a sensor and fast subsystem observer to detect the actuators' high-frequency dynamics. The slow and fast controllers are designed independently parameterized by a single parameter ε for time scale separation. Experimental results

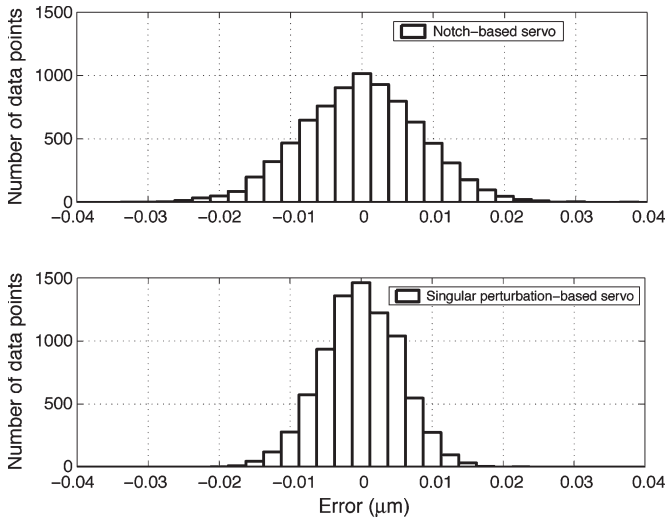

Fig. 21. Histograms of experimental PES y measured with LDV using disturbance and noise models described in [10]. Top: conventional notch-based servo. Bottom: proposed SP-based servo.

show an effective suppression of the VCM's flexible modes at 3.9 and 6.0 kHz, as well as the PZT active suspension's flexible modes at 5.9, 11.5, and 21.0 kHz with an improvement of 39.9% in 3σ PES during track-following. Future works include extending the current work to dual-stage HDDs using SSA [3] with an SP observer.

ACKNOWLEDGMENT

The authors would like to thank F. Hong of the A*STAR Data Storage Institute and M. Kobayashi of Central Research Laboratory, Hitachi, Ltd., for their valuable suggestions.

REFERENCES

[1] F. Y. Huang, W. Imaino, F. Lee, and T. Semba, "Active damping in HDD actuator," *IEEE Trans. Magn.*, vol. 37, no. 2, pp. 847–849, Mar. 2001.
[2] Y. Li, R. Horowitz, and R. Evans, "Vibration control of a PZT actuated suspension dual-stage Servo system using a PZT sensor," *IEEE Trans. Magn.*, vol. 39, no. 2, pp. 932–937, Mar. 2003.
[3] C. K. Pang, G. Guo, B. M. Chen, and T. H. Lee, "Self-sensing actuation for nanopositioning and active-mode damping in dual-stage HDDs," *IEEE/ASME Trans. Mechatronics*, vol. 11, no. 3, pp. 328–338, Jun. 2006.
[4] P. V. Kokotović, H. K. Khalil, and J. O'Reilly, *Singular Perturbation Methods in Control: Analysis and Design*. London, U.K.: Academic, 1986.
[5] F. L. Lewis, S. Jagannathan, and A. Yeşildirek, *Neural Network Control of Robot Manipulators and Nonlinear Systems*. London, U.K.: Taylor & Francis, 1999.
[6] M. Hirata, T. Atsumi, A. Murase, and K. Nonami, "Following control of a hard disk drive by using sampled-data $\mathcal{H}_\infty$ control," in *Proc. IEEE Int. CCA*, Kohala Coast-Island Hawaii, HI, Aug. 22–26, 1999, pp. 182–186.
[7] Y. Yamamoto and P. P. Khargonekar, "Frequency response of sampled-data systems," *IEEE Trans. Autom. Control*, vol. 41, no. 2, pp. 166–176, Feb. 1996.
[8] M. Araki, Y. Ito, and T. Haiwara, "Frequency response of sampled-data systems," *Automatica*, vol. 32, no. 4, pp. 483–497, Apr. 1996.
[9] *Nano Scale Servo*, Sep. 2006, Tokyo, Japan: Univ. Tokyo. (in Japanese). [Online]. Available: http://mizugaki.iis.u-tokyo.ac.jp/nss/
[10] C. Du, L. Xie, G. Guo, J. Zhang, Q. Li, B. Hredzak, and J. N. Teoh, "A generalized KYP lemma based control design and application for 425 kTPI servo track writing," in *Proc. ACC*, Minneapolis, MN, Jun. 14–16, 2006, pp. 1303–1308.
[11] C. K. Pang, D. Wu, G. Guo, T. C. Chong, and Y. Wang, "Suppressing sensitivity hump in HDD dual-stage servo systems," *Microsyst. Technol.*, vol. 11, no. 8–10, pp. 653–662, Aug. 2005.
[12] B. M. Chen, T. H. Lee, K. Peng, and V. Venkataramanan, *Hard Disk Drive Servo Systems*, 2nd ed. New York: Springer-Verlag, 2006.
[13] G. Cheng, K. Peng, B. M. Chen, and T. H. Lee, "Improving transient performance in tracking general references using composite nonlinear feedback control and its application to XY-table positioning mechanism," *IEEE Trans. Ind. Electron.*, to be published.
[14] S. S. Ge, T. H. Lee, F. Hong, and C. H. Goh , "Energy-based robust controller design for flexible spacecraft," *J. Control Theory Appl.*, vol. 2, no. 1, pp. 27–34, 2004.
[15] S. S. Ge, "Adaptive controller design for flexible joint manipulators," *Automatica*, vol. 32, no. 2, pp. 273–278, Feb. 1996.
[16] H. Fujimoto, Y. Hori, and A. Kawamura, "Perfect tracking control based on multirate feedforward control with generalized sampling periods," *IEEE Trans. Ind. Electron.*, vol. 48, no. 3, pp. 636–644, Jun. 2001.
[17] M. Kobayashi, S. Nakagawa, and S. Nakamura, "A phase-stabilized servo controller for dual-stage actuators in hard disk drives," *IEEE Trans. Magn.*, vol. 39, no. 2, pp. 844–850, Mar. 2003.
[18] P. V. Kokotović, "Applications of singular perturbation techniques to control problems," *SIAM Rev.*, vol. 26, no. 4, pp. 501–550, Oct. 1984.
[19] H. S. Lee, "Controller optimization for minimum position error signals of hard disk drives," *IEEE Trans. Ind. Electron.*, vol. 48, no. 5, pp. 945–950, Oct. 2001.
[20] F. L. Lewis, *Applied Optimal Control & Estimation*. Englewood Cliffs, NJ: Prentice-Hall, 1992.
[21] D. Wu, G. Guo, and T. C. Chong, "Comparative analysis on resonance compensation in HDD dual-stage actuation systems," *IEEE Trans. Ind. Electron.*, vol. 50, no. 6, pp. 1179–1186, Dec. 2003.

Chee Khiang Pang (S'04–M'07) was born in Singapore in 1976. He received the B.Eng. (Hons.) and M.Eng. degrees in electrical and computer engineering from the National University of Singapore (NUS), Singapore, in 2001 and 2003, respectively, where he is currently working toward the Ph.D. degree.

From February to June 2003, he was a Visiting Scholar with the School of Information Technology and Electrical Engineering, University of Queensland, Brisbane, Australia. Since April 2006, he has been with the Storage Technology Research Center, Central Research Laboratory, Hitachi, Ltd., Kanagawa, Japan. His current research interests include vibration analysis and servo control in sampled-data mechatronics, multisensing and active control in HDDs, and the self servo-track writing (SSW) process.

Frank L. Lewis (S'78–M'81–SM'86–F'94) received the Bachelor's degree in physics/electrical engineering and the M.S.E.E. degree from Rice University, Houston, TX, the M.S. degree in aeronautical engineering from the University Western Florida, Pensacola, and the Ph.D. from Georgia Institute of Technology, Atlanta.

He is a Distinguished Scholar Professor and Moncrief-O'Donnell Chair with the Automation and Robotics Research Institute, University of Texas at Arlington. He works in feedback control, intelligent systems, and sensor networks. He is the author of five U.S. patents, 174 journal papers, 286 conference papers, and 11 books.

Dr. Lewis is a Fellow of the U.K. Institute of Measurement and Control, a Registered Professional Engineer in the State of Texas, and a U.K. Chartered Engineer. He received the Fulbright Research Award, NSF Research Initiation Grant, and ASEE Terman Award. He also received an Outstanding Service Award from the Dallas IEEE Section and was selected as the Engineer of the Year by the Ft. Worth IEEE Section. He was listed in the Ft. Worth Business Press Top 200 Leaders in Manufacturing. He was appointed to the NAE Committee on Space Station in 1995. He is an elected Guest Consulting Professor at both South China University of Technology, Guangzhou, China, and Shanghai Jiao Tong University, Shanghai, China. He is a Founding Member of the Board of Governors of the Mediterranean Control Association. He helped win the IEEE Control Systems Society Best Chapter Award (as Founding Chairman of the DFW Chapter), the National Sigma Xi Award for Outstanding Chapter (as President of the UTA Chapter), and the U.S. SBA Tibbets Award in 1996 (as Director of ARRI's SBIR Program).

Shuzhi Sam Ge (S'90–M'92–SM'00–F'06) received the B.Sc. degree from Beijing University of Aeronautics and Astronautics (BUAA), Beijing, China, and the Ph.D. degree and the Diploma of Imperial College (DIC) from Imperial College of Science, Technology and Medicine, London, U.K.

He is a Professor with the Department of Electrical and Computer Engineering, National University of Singapore, Singapore. He has (co)-authored three books: *Adaptive Neural Network Control of Robotic Manipulators* (World Scientific, 1998), *Stable Adaptive Neural Network Control* (Kluwer, 2001), and *Switched Linear Systems: Control and Design* (Springer-Verlag, 2005), and over 300 international journal and conference papers. His current research interests include interactive robotics, adaptive control, and intelligent systems.

Dr. Ge has served/been serving as an Associate Editor for a number of flagship journals, including the IEEE TRANSACTIONS ON AUTOMATIC CONTROL, IEEE TRANSACTIONS ON CONTROL SYSTEMS TECHNOLOGY, IEEE TRANSACTIONS ON NEURAL NETWORKS, and *Automatica*. He also serves as an Editor of the Taylor & Francis Automation and Control Engineering Series.

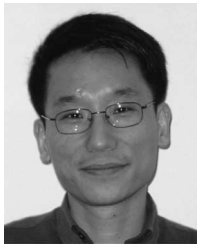

Guoxiao Guo (S'95–M'96–SM'05) received the B.Eng. and M.Eng. degrees from the Department of Automation, Tsinghua University, Beijing, China, in 1989 and 1994, respectively, and and the Ph.D. degree from the School of Electrical and Electronic Engineering, Nanyang Technological University, Singapore, in 1997.

In 1995, he joined the A*STAR Data Storage Institute, Singapore, as a Research Engineer and later became the Manager of the Mechatronics and Recording Channel Division. He is also an Adjunct Fellow with the National University of Singapore, Singapore, and an Adjunct Associate Professor with Nanyang Technological University. His research focuses on vibration analysis, sensing and control, mechatronics and MEMs, nonlinear and robust control for achieving nanopositioning systems in ultrahigh density magnetic recording. He has published over 50 refereed journal papers and six patents on these topics.

Dr. Guo was the Publication Chairman/Cochair for the Asia-Pacific Magnetic Recording Conferences held in Tokyo, Japan, in 2000, and in Singapore, in 2002, and in Seoul, Korea, in 2004, all focused on the mechanical and manufacturing aspects of magnetic recording systems. Since June 2005, he has been an Associate Editor of the IEEE TRANSACTIONS ON CONTROL SYSTEMS TECHNOLOGY.

Ben M. Chen (S'89–M'91–SM'00–F'07) was born in Fuqing, Fujian, China, in 1963. He received the B.S. degree in computer science and mathematics from Xiamen University, Xiamen, China, in 1983, the M.S. degree in electrical engineering from Gonzaga University, Spokane, WA, in 1988, and the Ph.D. degree in electrical and computer engineering from Washington State University, Pullman, in 1991.

From 1992 to 1993, he was an Assistant Professor with the Electrical Engineering Department, State University of New York at Stony Brook. Since 1993, he has been with the Department of Electrical and Computer Engineering, National University of Singapore, Singapore, where he is currently a Professor. His current research interests are in robust control, systems theory, and control applications. He is the author/coauthor of seven research monographs, including *Hard Disk Drive Servo Systems* (Springer, 1st Edition 2002, 2nd Edition 2006); *Linear Systems Theory: A Structural Decomposition Approach* (Birkhäuser, 2004); and *Robust and H_∞ Control* (Springer, 2000).

Dr. Chen was an Associate Editor for the IEEE TRANSACTIONS ON AUTOMATIC CONTROL. He was an Associate Editor for *Asian Journal of Control*, and is currently serving as an Associate Editor of *Automatica, Control and Intelligent Systems* and *Systems and Control Letters*.

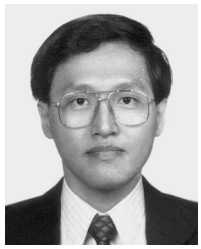

Tong Heng Lee (M'90) received the B.A. degree (with First Class Honors) in engineering tripos from Cambridge University, Cambridge, U.K., in 1980, and the Ph.D. degree from Yale University, New Haven, CT, in 1987.

He is a Professor with the Department of Electrical and Computer Engineering, National University of Singapore, Singapore. His research interests are in the areas of adaptive systems, knowledge-based control, intelligent mechatronics, and computational intelligence. He has also coauthored three research monographs, and holds four patents (two of which are in the technology area of adaptive systems, and the other two are in the area of intelligent mechatronics).

Dr. Lee is currently an Associate Editor for *Automatica*; the IEEE TRANSACTIONS ON SYSTEMS, MAN AND CYBERNETICS; *Control Engineering Practice*; the *International Journal of Systems Science*; and *Mechatronics Journal*. He was a recipient of the Cambridge University Charles Baker Prize in Engineering.